ELSEVIER

1 June 1997

Optics Communications 138 (1997) 394–402

OPTICS COMMUNICATIONS

Full length article

Diffraction analysis of pixelated incoherent shadow casting

Vincent Laude [1]

Thomson-CSF, Laboratoire Central de Recherches, F-91404 Orsay Cedex, France

Received 10 December 1996; revised 10 February 1997; accepted 13 February 1997

Abstract

Discrete incoherent shadow-casting systems are investigated under the Fresnel scalar approximation of diffraction. Shadow casting systems are non-imaging optical systems used in optical information processing, that are made basically of a spatially incoherent diffuse source plane, an intermediate filter plane and a detection plane. The analysis assumes that these three planes are pixelated, e.g. because of the use of electrically addressed spatial light modulators and a CCD camera. A model is derived relating the output image in the detection plane to the two input images in the source and intermediate planes. This model explicitly involves the shadow of the intermediate plane projected by the source plane onto the detection plane. It can be used to obtain a precise evaluation of the diffraction limited resolution available for information processing and is the basis for numerical simulation of shadow casting systems.

Keywords: Shadow casting; Incoherent correlation; Incoherent optical information processing

1. Introduction

Shadow casting optical systems have been used for information processing for more than fifty years, and were first used as correlators [1,2], as they provide a very simple way of measuring the correlation or convolution product of two images, without the need for Fourier transform lenses [3]. Furthermore, shadow casting has been used for the optical implementation of a variety of applications, including digital computing [4], morphological processing [5], and symbolic substitution [6] among others. Since they assume spatially incoherent illumination, shadow casting systems are robust to misalignments and imperfections of optical elements compared with coherent systems [7], and do not require a laser source. However, with the advent of coherent optical information processing in the late sixties, shadow casting as well as incoherent information processing in general declined. The main limitation of shadow casting that is classically accounted for following Green [8], whose analysis is based on the number of degrees of freedom in a optical beam, is that diffraction limits severely the resolution available for processing. It is our belief that, although the analysis of Ref. [8] is correct within its scope, there are some geometrical configurations for shadow casting that are less limited in resolution by diffraction than is usually believed. First steps in that direction were taken by Raj et al. [9,10] and by Gedziorowski et al. [11], who respectively showed the resolution enhancement that can be gained by using a dilute light source array and by taking into account the fact that the illumination is partially coherent in the plane where diffraction occurs.

Recent implementations of shadow casting [12,13] rely on pixelated spatial light modulators (SLM), e.g. liquid crystal televisions (LCTV), for displaying input images, and on CCD cameras for output detection. In this paper, we tackle the problem of estimating the diffraction limited resolution of shadow casting from the assumption that modulation and detection planes are pixelated, and by subsequently deriving a discrete relation expressing the output image as the correlation (or convolution) of the first input image with the shadow of the second image cast onto the detection plane. This relation is derived in two steps,

[1] E-mail: laude@thomson-lcr.fr.

PII S0030-4018(97)00088-6

first within the geometrical optics approximation, then within the Fresnel scalar approximation of diffraction [14]. It is valid whatever the pixels shape and spacing, and allows for an exact (within the Fresnel approximation) and efficient numerical simulation of pixelated shadow casting systems. Furthermore, previous assessments of the resolution of shadow casting are included in our model in the limit that resolution cells can be approximated as pixels.

The paper is organized as follows. We first recall the basic properties of shadow casting in Section 2. We investigate pixelated shadow casting systems within the geometrical optics approximation in Section 3 and then within the Fresnel approximation of diffraction in Section 4. Next, the common case of rectangular pixels is considered in Section 5. A simple quantitative criterion for resolution assessment is derived is this case, and simulation and experimental results are presented.

2. Shadow casting basics

The simplest shadow casting system is depicted in Fig. 1. It is lensless, and basically involves three planes. The first plane, denoted $\mathscr{P}_1$, is a diffuse spatially incoherent source, that can be e.g. a CRT [15], a LED array [9,10], or even a transparency or a SLM followed by a diffuser [13]. The second plane $\mathscr{P}_2$ at a distance d is a transparency or a SLM, and the third and last plane $\mathscr{P}_3$ at a distance p is a screen or a camera. This basic shadow casting system can be generalized [3,15,16] with the addition of lenses in between the three planes, as depicted in Fig. 2. However, considering the images of planes $\mathscr{P}_1$ and $\mathscr{P}_2$ through the lenses, we are led back to the lensless system of Fig. 1, at least within the geometrical optics and Fresnel approximations that will be used in this paper. Only the lensless case will be considered from now on. It is worth noting that both distances d and p can be positive or negative, or even infinite.

The principle of shadow casting can be understood in

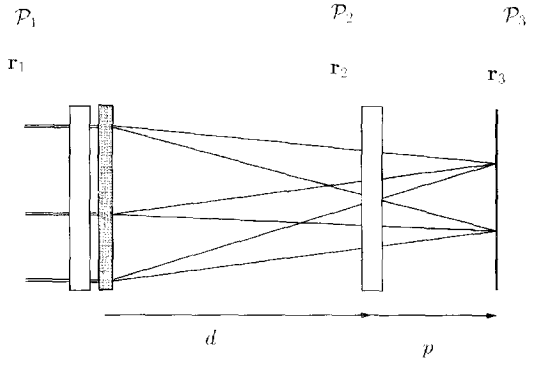

Fig. 1. Lensless shadow casting.

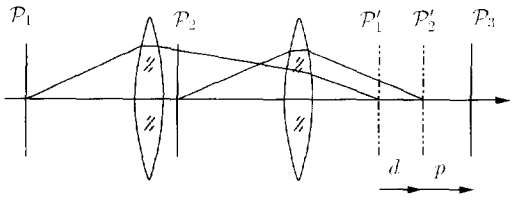

Fig. 2. General shadow casting with lenses.

terms of ray optics. With the notations of Fig. 1, a ray emitted from point $\boldsymbol{r}_1$ in the source plane and arriving at point $\boldsymbol{r}_3$ in the detection plane crosses the second plane at point $\boldsymbol{r}_2$ such that

$$\frac{\boldsymbol{r}_2}{d'} = \frac{\boldsymbol{r}_1}{d} + \frac{\boldsymbol{r}_3}{p}, \tag{1}$$

where the algebraic distance d' is defined as

$$\frac{1}{d'} = \frac{1}{d} + \frac{1}{p}. \tag{2}$$

Considering the elementary surfaces $\mathrm{d}\boldsymbol{r}_1$ and $\mathrm{d}\boldsymbol{r}_3$ centered at points $\boldsymbol{r}_1$ and $\boldsymbol{r}_3$, both the source and the optical system can be characterized by the elementary flux $\xi(\boldsymbol{r}_1,\boldsymbol{r}_3)\mathrm{d}\boldsymbol{r}_1\,\mathrm{d}\boldsymbol{r}_3$ that is emitted at $\mathrm{d}\boldsymbol{r}_1$ and received in $\mathrm{d}\boldsymbol{r}_3$. The irradiance is then given by the contribution of all source elements

$$E(\boldsymbol{r}_3) = \int_{\mathscr{P}_1} \mathrm{d}\boldsymbol{r}_1\, \xi(\boldsymbol{r}_1,\boldsymbol{r}_3)\, T_1(\boldsymbol{r}_1)\, T_2\left(d'\left(\frac{\boldsymbol{r}_1}{d} + \frac{\boldsymbol{r}_3}{p}\right)\right), \tag{3}$$

where T_1 and T_2 are the intensity transmittances in planes $\mathscr{P}_1$ and $\mathscr{P}_2$. Eq. (3) shows that the operation achieved by shadow casting is, in terms of ray optics, a bilinear transformation with a positive kernel ξ of two positive functions T_1 and T_2. The kernel ξ describes the photometric properties of the system, and depends on the source, diaphragms and lenses used. It needs to be constant for correlation or convolution. Let us define $\gamma = |d'/d|$, and the signs ϵ and ϵ' of d'/d and d'/p respectively. We then have $|d'/p| = |\gamma - \epsilon|$. With these definitions, Eq. (3) can be written as

$$E(\boldsymbol{r}_3) = \int_{\mathscr{P}_1} \mathrm{d}\boldsymbol{r}_1\, \xi(\boldsymbol{r}_1,\boldsymbol{r}_3)\, T_1(\boldsymbol{r}_1)\, T_2\big(\epsilon\gamma\boldsymbol{r}_1 + \epsilon'|\gamma - \epsilon|\boldsymbol{r}_3\big). \tag{4}$$

We also define $G = 1/\gamma$ for accordance with Ref. [13]. G is the dilation factor of function T_1 with respect to function T_2. It can be seen from Eq. (4) that if $\epsilon = 1$ (respectively $\epsilon = -1$) the correlation (respectively convolution) of a scaled version of T_1 with T_2 is obtained. If $\epsilon' = -1$, the correlation or convolution is observed inverted with respect to the origin of plane P_3.

3. Discrete geometrical analysis

We now consider pixelated shadow casting systems. We want to emphasize that even though the propagation of light must be treated using continuous functions, namely the complex amplitude of the wave in the scalar diffraction theory, the input to a pixelated SLM and the output from a CCD camera are discrete images, and information is processed as such in a pixelated shadow casting system. As a first step we investigate in this section properties of pixelated shadow casting in the approximation of ray optics.

3.1. Notations

As depicted in Fig. 3, in each of the three planes $\mathscr{P}_i$ ($i = 1,2,3$) an elementary pixel function $p_i(\boldsymbol{r}_i)$ is repeated on a rectangular grid with pitch $\boldsymbol{b}_i$. Pixel functions $p_i(\boldsymbol{r}_i)$ are functions representing apertures. Note that physical pixels in the same plane, and hence pixel functions, do not overlap. For instance, rectangular pixels can be written as $p_i(\boldsymbol{r}_i) = \mathrm{rect}(x_i/a_{ix})\mathrm{rect}(y_i/a_{iy})$, where $\mathrm{rect}(t)$ equals 1 if $-1/2 \le t \le 1/2$ and 0 otherwise, and $\boldsymbol{a}_i$ is the width of the pixels. We also introduce dimensionless coordinates by defining $\boldsymbol{R}_i$ as the vector with coordinates $X_i = x_i/b_{ix}$ and $Y_i = y_i/b_{iy}$. Note that the pixel function $p_i(\boldsymbol{r}_i)$ needs not necessarily correspond to a single physical pixel of a SLM, CRT or CCD array. Physical pixels in these devices might be grouped, for instance by 2×2, to yield the meta pixel $p_i(\boldsymbol{r}_i)$.

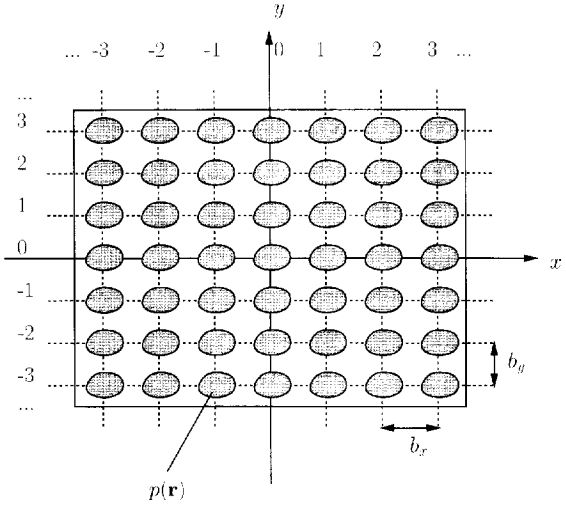

Fig. 3. Structure of each of the three pixelated planes. The elementary pixel function $p_i(\boldsymbol{r}_i)$ ($i = 1,2,3$) is repeated periodically on a rectangular grid with pitch $\boldsymbol{b}_i$. Pixels are numbered from the optical axis.

With these notations, we can write transmittance T_1 as

$$T_1(\boldsymbol{R}_1) = \sum_{m_y=-M_y}^{M_y} \sum_{m_x=-M_x}^{M_x} T_1(\boldsymbol{m})\, p_1(\boldsymbol{R}_1 - \boldsymbol{m}), \tag{5}$$

or in short

$$T_1(\boldsymbol{R}_1) = \sum_{\boldsymbol{m}} T_1(\boldsymbol{m})\, p_1(\boldsymbol{R}_1 - \boldsymbol{m}). \tag{6}$$

The input image is supposed to be of size $(2M_x + 1) \times (2M_y + 1)$ pixels, and pixels are numbered from the optical axis. The quantity $T_1(\boldsymbol{m})$ is the intensity transmission at pixel $\boldsymbol{m}$, and is always smaller than 1. Similarly we can write for transmittance T_2

$$T_2(\boldsymbol{R}_2) = \sum_{\boldsymbol{n}} T_2(\boldsymbol{n})\, p_2(\boldsymbol{R}_2 - \boldsymbol{n}), \tag{7}$$

where the second image is assumed to be of size $(2N_x + 1) \times (2N_y + 1)$ pixels. In the detection plane, the output image is denoted Φ_3. It is assumed to be of size $(2K_x + 1) \times (2K_y + 1)$ pixels and can be written

$$\Phi_3(\boldsymbol{k}) = S_3 \int_{\mathscr{P}_3} \mathrm{d}\boldsymbol{R}_3\, E(\boldsymbol{R}_3)\, p_3(\boldsymbol{R}_3 - \boldsymbol{k}), \tag{8}$$

i.e. $\Phi_3(\boldsymbol{k})$ is the flux received by detection pixel number $\boldsymbol{k}$. The irradiance E is now expressed as a function of $\boldsymbol{R}_3$ instead of $\boldsymbol{r}_3$. S_3 is the surface defined by $S_3 = b_{3x}b_{3y}$. We define likewise the surfaces $S_1 = b_{1x}b_{1y}$ and $S_2 = b_{2x}b_{2y}$. Note that these surfaces are associated to the rectangular grids, and are in general different from the pixels surfaces defined as $Sp_i = S_i \int_{\mathscr{P}_i} \mathrm{d}\boldsymbol{R}_i\, p_i(\boldsymbol{R}_i)$.

3.2. Small pixels limit

Let us first consider that the pixels in the three planes are very small, or point-like. Obviously this is an unrealistic situation, since less and less light will be available for detection as the pixels become smaller. We write $p_i(\boldsymbol{R}_i) = (Sp_i/S_i)\delta(\boldsymbol{R}_i)$ where the pixel surface Sp_i is very small and $\delta(\,)$ denotes the Dirac function. We define the product $\boldsymbol{u} \odot \boldsymbol{v}$ of two vectors $\boldsymbol{u}$ and $\boldsymbol{v}$ as the vector with coordinates $(u_x v_x, u_y v_y)$. With these definitions, Eq. (4) becomes

$$E(\boldsymbol{R}_3) = Sp_1 \frac{Sp_2}{S_2} \sum_{\boldsymbol{m}} T_1(\boldsymbol{m}) \sum_{\boldsymbol{n}} T_2(\boldsymbol{n})\, \xi(\boldsymbol{m}, \boldsymbol{R}_3) \times \delta\big(\epsilon\gamma \boldsymbol{b}_{12} \odot \boldsymbol{m} + \epsilon' |\gamma - \epsilon| \boldsymbol{b}_{32} \odot \boldsymbol{R}_3 - \boldsymbol{n}\big), \tag{9}$$

and Eq. (8) becomes

$$\Phi_3(\boldsymbol{k}) = Sp_3\, E(\boldsymbol{k}),$$

$$\Phi_3(\boldsymbol{k}) = Sp_1 \frac{Sp_2}{S_2} Sp_3 \sum_{\boldsymbol{m}} T_1(\boldsymbol{m}) \sum_{\boldsymbol{n}} T_2(\boldsymbol{n}) \xi(\boldsymbol{m}, \boldsymbol{k}) \times \delta\big(\epsilon\gamma \boldsymbol{b}_{12} \odot \boldsymbol{m} + \epsilon' |\gamma - \epsilon| \boldsymbol{b}_{32} \odot \boldsymbol{k} - \boldsymbol{n}\big). \tag{10}$$

If all information contained in the input images is to be used in the discrete shadow casting system, to every input images pixels $\boldsymbol{m}$ and $\boldsymbol{n}$ must be associated an output pixel $\boldsymbol{k}$ such that

$$\boldsymbol{n} = \epsilon\gamma \boldsymbol{b}_{12} \odot \boldsymbol{m} + \epsilon' |\gamma - \epsilon| \boldsymbol{b}_{32} \odot \boldsymbol{k}. \tag{11}$$

Eq. (11) is the discrete counterpart of Eq. (1), and implies that

$$\boldsymbol{b}_2 = \gamma \boldsymbol{b}_1 = |\gamma - \epsilon| \boldsymbol{b}_3. \tag{12}$$

This amounts to say that the three rectangular grids are identical except for a scale factor. When the pixel pitch is chosen in two planes, the third is imposed by Eq. (12). Eq. (11) then simplifies to

$$\boldsymbol{n} = \epsilon\, \boldsymbol{m} + \epsilon'\, \boldsymbol{k}, \tag{13}$$

which expresses the geometrical relation between pixels, and Eq. (10) simplifies to

$$\Phi_3(\boldsymbol{k}) = Sp_1 \frac{Sp_2}{S_2} Sp_3 \sum_{\boldsymbol{m}} \xi(\boldsymbol{m},\boldsymbol{k})\, T_1(\boldsymbol{m})\, T_2(\epsilon\, \boldsymbol{m} + \epsilon'\, \boldsymbol{k}). \tag{14}$$

This is a discrete version of Eq. (4), in the form of a bilinear discrete transformation.

3.3. General geometrical expression

Let us now extend the previous results to arbitrarily shaped pixels. We assume from now on that the condition of Eq. (11) holds. The irradiance of Eq. (4) can be written using Eqs. (6) and (7)

$$E(\boldsymbol{R}_3) = \sum_{\boldsymbol{m}} T_1(\boldsymbol{m}) \sum_{\boldsymbol{n}} T_2(\boldsymbol{n})\, S_1 \int_{\mathscr{P}_1} \mathrm{d}\boldsymbol{R}_1\, \xi(\boldsymbol{R}_1,\boldsymbol{R}_3) \times p_1(\boldsymbol{R}_1 - \boldsymbol{m})\, p_2(\epsilon \boldsymbol{R}_1 + \epsilon' \boldsymbol{R}_3 - \boldsymbol{n}), \tag{15}$$

where kernel ξ is now expressed as a function of the reduced coordinates $\boldsymbol{R}_1$ and $\boldsymbol{R}_3$ instead of $\boldsymbol{r}_3$ and $\boldsymbol{r}_1$ respectively. Eq. (8) then becomes

$$\Phi_3(\boldsymbol{k}) = \sum_{\boldsymbol{m}} T_1(\boldsymbol{m}) \sum_{\boldsymbol{n}} T_2(\boldsymbol{n})\, S_1 S_3 \int_{\mathscr{P}_1} \mathrm{d}\boldsymbol{R}_1 \times \int_{\mathscr{P}_3} \mathrm{d}\boldsymbol{R}_3\, \xi(\boldsymbol{R}_1,\boldsymbol{R}_3)\, p_1(\boldsymbol{R}_1 - \boldsymbol{m}) \times p_3(\boldsymbol{R}_3 - \boldsymbol{k})\, p_2(\epsilon \boldsymbol{R}_1 + \epsilon' \boldsymbol{R}_3 - \boldsymbol{n}). \tag{16}$$

We assume that the function ξ, that represents the photometric properties of the system, varies very slowly at the scale of the pixel pitches, so that $\xi(\boldsymbol{R}_1,\boldsymbol{R}_3)$ can be replaced by $\xi(\boldsymbol{m},\boldsymbol{k})$ within pixels $\boldsymbol{m}$ and $\boldsymbol{k}$. This a quite general assumption in shadow-casting systems provided the pixels are small enough. Defining the elementary flux

$$Q(\boldsymbol{m},\boldsymbol{k}) = S_1 S_3\, \xi(\boldsymbol{m},\boldsymbol{k}), \tag{17}$$

that is representative of the light power contained in the particular channel linking emitting pixel $\boldsymbol{m}$ to detection pixel $\boldsymbol{k}$, we can write

$$\Phi_3(\boldsymbol{k}) = \sum_{\boldsymbol{m}} T_1(\boldsymbol{m}) \sum_{\boldsymbol{n}} T_2(\boldsymbol{n})\, Q(\boldsymbol{m},\boldsymbol{k}) \int_{\mathscr{P}_1} \mathrm{d}\boldsymbol{R}_1 \times \int_{\mathscr{P}_3} \mathrm{d}\boldsymbol{R}_3\, p_1(\boldsymbol{R}_1)\, p_3(\boldsymbol{R}_3) \times p_2(\epsilon(\boldsymbol{R}_1 + \boldsymbol{m}) + \epsilon'(\boldsymbol{R}_3 + \boldsymbol{k}) - \boldsymbol{n}). \tag{18}$$

Upon introducing

$$\boldsymbol{q} = \boldsymbol{n} - \epsilon\, \boldsymbol{m} - \epsilon'\, \boldsymbol{k}, \tag{19}$$

Eq. (18) can be written

$$\Phi_3(\boldsymbol{k}) = \sum_{\boldsymbol{m}} Q(\boldsymbol{m},\boldsymbol{k})\, T_1(\boldsymbol{m})\, G[T_2](\epsilon\, \boldsymbol{m} + \epsilon'\, \boldsymbol{k}), \tag{20}$$

$$G[T_2](\boldsymbol{n}) = \sum_{\boldsymbol{q}} A(\boldsymbol{q})\, T_2(\boldsymbol{n} + \boldsymbol{q}), \tag{21}$$

$$A(\boldsymbol{q}) = \int_{\mathscr{P}_1} \mathrm{d}\boldsymbol{R}_1 \int_{\mathscr{P}_3} \mathrm{d}\boldsymbol{R}_3\, p_1(\boldsymbol{R}_1)\, p_3(\boldsymbol{R}_3) \times p_2(\epsilon \boldsymbol{R}_1 + \epsilon' \boldsymbol{R}_3 - \boldsymbol{q}). \tag{22}$$

Eqs. (20)–(22) are a generalization of Eq. (14) for arbitrarily shaped pixel functions in the approximation of ray optics. The discrete bilinear transform now involves the 'blurred' image $G[T_2]$ instead of simply T_2. Coefficients $A(\boldsymbol{q})$ are dimensionless and positive, and are such that $\Sigma_{\boldsymbol{q}} A(\boldsymbol{q}) \leq 1$, and equal to 0 as soon as $|q_x|$ or $|q_y|$ is greater than 1. Thus, $G[T_2]$ is the result of a low-pass filtering of image T_2 with a blurring kernel of size 3×3. Quite intuitively, the maximum blur with a rectangular pixel is obtained when

$$p_i(\boldsymbol{R}_i) = \mathrm{rect}(\boldsymbol{R}_i), \quad i = 1,2,3. \tag{23}$$

In this case, it is easy to show that

$$A = \begin{pmatrix} 1/64 & 6/64 & 1/64 \\ 6/64 & 36/64 & 6/64 \\ 1/64 & 6/64 & 1/64 \end{pmatrix}, \tag{24}$$

and in this case only $\Sigma_{\boldsymbol{q}} A(\boldsymbol{q}) = 1$. Anyway, this geometrical blurring effect is in general not very important when compared to diffraction effects, and does not reduce significantly the output resolution.

4. Diffraction analysis

We now investigate in this section properties of pixelated shadow casting in the Fresnel approximation of diffraction.

4.1. Incoherent point spread function

The spatial incoherence assumption in the source plane amounts to considering all source points as independent.

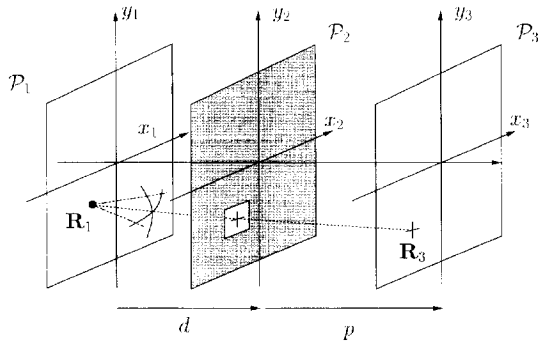

Fig. 4. Diffraction of a spherical wave by a pixel of plane $\mathscr{P}_2$.

The spherical wave emitted at point $\boldsymbol{R}_1$ of plane $\mathscr{P}_1$ is diffracted by the pixels of plane $\mathscr{P}_2$, as depicted in Fig. 4. The Fresnel approximation of diffraction [17,14] that we use is valid in the paraxial domain and if the pixels of the second plane are larger than the wavelength. As is detailed in Appendix A, the incoherent point spread function (PSF) is given by

$$H_\lambda(\boldsymbol{R}_1,\boldsymbol{R}_3) = \left| \sum_{\boldsymbol{n}} t_2(\boldsymbol{n})\, F_\lambda(\epsilon \boldsymbol{R}_1 + \epsilon' \boldsymbol{R}_3 - \boldsymbol{n}) \right|^2 . \tag{25}$$

where the summation on $\boldsymbol{n}$ extends over all pixels of the second plane, and

$$F_\lambda(\boldsymbol{U}) = \frac{S_2}{\lambda |d'|} \int_{\mathscr{P}_2} \mathrm{d}\boldsymbol{R}_2\; p_2(\boldsymbol{R}_2) \exp\left(\frac{i\pi b_{2x}^2}{\lambda d'} (X_2 - U_x)^2 \right) \times \exp\left(\frac{i\pi b_{2y}^2}{\lambda d'} (Y_2 - U_y)^2 \right), \tag{26}$$

is the complex amplitude of the Fresnel coherent PSF describing the diffraction by a single pixel of plane $\mathscr{P}_2$ centered on the optical axis. This formulation is based on the translational invariance that is a consequence of the Fresnel approximation: if the source point or the diffracting pixel is displaced, the PSF remains the same but is displaced according to the laws of ray optics. The shape of the PSF depends on the wavelength λ, hence the subscript in F_λ and H_λ. The PSFs of all pixels in plane $\mathscr{P}_2$ add coherently since they describe the diffraction of the same spherical wave. Note that the amplitude transmission $t_2(\boldsymbol{n})$ is involved rather than the intensity transmission $T_2(\boldsymbol{n}) = |t_2(\boldsymbol{n})|^2$ as in the geometrical analysis of the previous section. It must be stressed also that the amplitude transmission $t_2(\boldsymbol{n})$ can depend on the wavelength, e.g. this is the case for a liquid crystal SLM.

4.2. Input–output relation

In the previous section we did not consider the spectral content of the source. However, the incoherent PSF depends obviously on the wavelength λ. For simplicity, we consider only the two extreme cases of temporally incoherent and coherent sources. The output image of Eq. (8) can be written

$$\Phi_3(\boldsymbol{k}) = S_3 \int B(\lambda)\, \mathrm{d}\lambda \int_{\mathscr{P}_3} E_\lambda(\boldsymbol{R}_3)\, p_3(\boldsymbol{R}_3 - \boldsymbol{k})\, \mathrm{d}\boldsymbol{R}_3 , \tag{27}$$

where $B(\lambda)$ is the spectrum of a temporally incoherent source, and by convention $B(\lambda) = \delta(\lambda - \lambda_0)$ if the source is quasi-monochromatic at wavelength λ_0. In both cases the function $B(\lambda)$ is normalized by

$$\int B(\lambda)\, \mathrm{d}\lambda = 1 . \tag{28}$$

The spectral irradiance E_λ is now given by

$$E_\lambda(\boldsymbol{R}_3) = S_1 \int_{\mathscr{P}_1} \mathrm{d}\boldsymbol{R}_1\; \xi(\boldsymbol{R}_1,\boldsymbol{R}_3)\, T_1(\boldsymbol{R}_1)\, H_\lambda(\boldsymbol{R}_1,\boldsymbol{R}_3) . \tag{29}$$

The flux $\xi(\boldsymbol{R}_1,\boldsymbol{R}_3)$ corrects the individual contribution of each information channel irrespectively of the actual path followed by the wave to propagate from point $\boldsymbol{R}_1$ to point $\boldsymbol{R}_3$. This approximation is only valid in the case of weak diffraction, i.e. if the Fresnel PSF does not differ too much from the geometrical shadow of a pixel of plane $\mathscr{P}_2$. This condition will be quantitatively discussed in the next section when we particularize our discussion to rectangular pixels. As is detailed in Appendix B, Eqs. (20)–(22) describing in the geometrical approximation the input–output relation can be expressed in the Fresnel approximation of diffraction as

$$\Phi_3(\boldsymbol{k}) = \sum_{\boldsymbol{m}} Q(\boldsymbol{m},\boldsymbol{k})\, T_1(\boldsymbol{m})\, D[t_2](\epsilon \boldsymbol{m} + \epsilon' \boldsymbol{k}), \tag{30}$$

$$D[t_2](\boldsymbol{n}) = \sum_{\boldsymbol{q}} \sum_{\boldsymbol{q}'} V(\boldsymbol{q},\boldsymbol{q}')\, t_2(\boldsymbol{n} + \boldsymbol{q})\, t_2^*(\boldsymbol{n} + \boldsymbol{q}'), \tag{31}$$

$$V(\boldsymbol{q},\boldsymbol{q}') = \int B(\lambda)\, \mathrm{d}\lambda \int_{\mathscr{P}_1} \mathrm{d}\boldsymbol{R}_1 \times \int_{\mathscr{P}_3} \mathrm{d}\boldsymbol{R}_3\; p_1(\boldsymbol{R}_1)\, p_3(\boldsymbol{R}_3) \times F_\lambda(\epsilon \boldsymbol{R}_1 + \epsilon' \boldsymbol{R}_3 - \boldsymbol{q})\, F_\lambda^*(\epsilon \boldsymbol{R}_1 + \epsilon' \boldsymbol{R}_3 - \boldsymbol{q}') . \tag{32}$$

These equations are the main result of this paper. Despite their apparent complexity, they convey a relatively simple physical meaning. The image $D[t_2]$ might be viewed as the *shadow* of image t_2 cast onto the detection pixels by a single source pixel, or equivalently as the discrete PSF of the system. The discrete input–output relation is a bilinear transform of images T_1 and $D[t_2]$. Coefficients $V(\boldsymbol{q},\boldsymbol{q}')$ that relate the shadow $D[t_2]$ to the amplitude image t_2

fully describe the effect of diffraction. They can be understood as follows. Given a source pixel $\boldsymbol{m}$ and a detection pixel $\boldsymbol{k}$, a ray joining their centers would go through pixel $\boldsymbol{n}$ of the second plane such that $\boldsymbol{n} = \epsilon \boldsymbol{m} + \epsilon' \boldsymbol{k}$. But as a result of diffraction, the interference of the waves that have gone respectively through the neighboring pixels $\boldsymbol{n} + \boldsymbol{q}$ and $\boldsymbol{n} + \boldsymbol{q}'$ are recorded by the detection pixel, and contribute proportionally to $2\Re\{V(\boldsymbol{q},\boldsymbol{q}')\, t_2(I_2(\boldsymbol{n} + \boldsymbol{q}))\, t_2^*(I_2(\boldsymbol{n} + \boldsymbol{q}'))\}$, where $\Re\{\}$ denotes the real part of a complex number. As $\boldsymbol{q}$ and $\boldsymbol{q}'$ become larger, $V(\boldsymbol{q},\boldsymbol{q}')$ becomes smaller and eventually vanishes. The extent of the 4D array V, defined by the values $V(\boldsymbol{q},\boldsymbol{q}')$ that are not negligible, measures the importance of diffraction, and then the effective resolution.

Eqs. (30)–(32) form the basis for an efficient numerical simulation of pixelated shadow casting systems, that is exact within the Fresnel approximation of diffraction. Practically, coefficients $V(\boldsymbol{q},\boldsymbol{q}')$ can be tabulated once for all for a given set-up, independently of images T_1 and t_2. Furthermore the computation of the shadow $D[t_2]$ is independent of image T_1. Eqs. (30) and (31) depend on the pixel shapes and geometries only through the coefficients $V(\boldsymbol{q},\boldsymbol{q}')$ as given by Eq. (32). More precisely the pixel shape in the intermediate plane has an influence only on the Fresnel coherent PSF F_λ; this particular function is given in textbooks for rectangular and circular apertures [17] and can be computed using standard methods for other pixel shapes [18]. The pixels shapes in the source and detection planes are required to integrate the Fresnel coherent PSF F_λ to obtain $V(\boldsymbol{q},\boldsymbol{q}')$ from Eq. (32); this integration is well-behaved and can be performed accurately using Simpson's rule for example [18].

Whatever the pixel functions $p_1(\boldsymbol{R}_1)$, $p_2(\boldsymbol{R}_2)$ and $p_3(\boldsymbol{R}_3)$, the coefficients $V(\boldsymbol{q},\boldsymbol{q}')$ are Hermitian symmetrical

$$V(\boldsymbol{q}',\boldsymbol{q}) = V^*(\boldsymbol{q},\boldsymbol{q}'). \tag{33}$$

Moreover, as shown in Appendix B, they identify with the geometrical coefficients $A(\boldsymbol{q})$ as the wavelength goes to 0

$$\begin{aligned} &\lim_{\lambda \to 0}[V(\boldsymbol{q},\boldsymbol{q})] = A(\boldsymbol{q}), \\ &\lim_{\lambda \to 0}[V(\boldsymbol{q},\boldsymbol{q}')] = 0 \quad \text{if } \boldsymbol{q}' \neq \boldsymbol{q}, \end{aligned} \tag{34}$$

and the following summations are independent of the wavelength

$$\begin{aligned} &\sum_{\boldsymbol{q}} V(\boldsymbol{q},\boldsymbol{q}) = \sum_{\boldsymbol{q}} A(\boldsymbol{q}), \\ &\sum_{\boldsymbol{q}} \sum_{\boldsymbol{q}' \neq \boldsymbol{q}} V(\boldsymbol{q},\boldsymbol{q}') = 0. \end{aligned} \tag{35}$$

5. Rectangular pixels

The special case of rectangular pixels is of great practical importance since it corresponds to the vast majority of electrically addressed SLMs and CCD cameras. This particularly simple shape leads to a quite simple computation of the diffraction coefficients $V(\boldsymbol{q},\boldsymbol{q}')$, and to quantitative rules for evaluating the diffraction limited resolution. If the pixels in plane $\mathscr{P}_2$ are rectangular, we can write

$$p_2(\boldsymbol{R}_2) = \mathrm{rect}\left(\frac{X_2}{\tau_{2x}}\right) \mathrm{rect}\left(\frac{Y_2}{\tau_{2y}}\right), \tag{36}$$

where parameters τ_{2x} and τ_{2y} measure the pixel fill factor. They are dimensionless, positive, smaller than 1, and obviously related to the pixel dimensions by $a_{2x} = \tau_{2x} b_{2x}$ and $a_{2y} = \tau_{2y} b_{2y}$. The rectangular pixel function is separable, a property which simplifies the following derivations. The Fresnel diffraction pattern of Eq. (26) becomes

$$\begin{aligned} F_\lambda(\boldsymbol{U}) = \frac{b_{2x} b_{2y}}{\lambda |d'|} &\int_{-\tau_{2x}/2}^{\tau_{2x}/2} \mathrm{d}X_2 \exp\left(\frac{i\pi b_{2x}^2}{\lambda d'}(X_2 - U_x)^2\right) \\ &\times \int_{-\tau_{2y}/2}^{\tau_{2y}/2} \mathrm{d}Y_2 \exp\left(\frac{i\pi b_{2y}^2}{\lambda d'}(Y_2 - U_y)^2\right). \end{aligned} \tag{37}$$

We define the Fresnel parameters α_x and α_y by

$$\alpha_x = \frac{\tau_{2x} b_{2x}}{\sqrt{\lambda |d'|}}, \quad \alpha_y = \frac{\tau_{2y} b_{2y}}{\sqrt{\lambda |d'|}}. \tag{38}$$

As will be seen later, these parameters are representative of the diffraction limited resolution. We also introduce the Fresnel integral defined by

$$\psi(\nu) = \int_0^\nu \exp(i\pi t^2)\, \mathrm{d}t. \tag{39}$$

This special function is tabulated in many books, or can be easily evaluated from its series and asymptotic expansions [19]. After some algebra, Eq. (37) can be written as

$$F_\lambda(\boldsymbol{U}) = \tau_{2x}\tau_{2y}\, \Delta\psi(\alpha_x, U_x/\tau_{2x})\, \Delta\psi(\alpha_y, U_y/\tau_{2y}), \tag{40}$$

with

$$\begin{aligned} &\Delta\psi(\alpha, U) = \psi(\alpha(U + 1/2)) - \psi(\alpha(U - 1/2)), \\ &\quad \text{if } \alpha \geq 0, \\ &\Delta\psi(\alpha, U) = \psi^*(|\alpha|(U + 1/2)) - \psi^*(|\alpha|(U - 1/2)), \\ &\quad \text{if } \alpha < 0. \end{aligned} \tag{41}$$

Eq. (40) yields a fast computation of the Fresnel PSF of a rectangular pixel. It depends only on the dimensionless parameters α_x, α_y, τ_{2x} and τ_{2y}.

Fig. 5 shows cross-sections of the squared modulus of F_λ for a rectangular pixel. When $\alpha = \infty$ the geometrical approximation of Section 3 is valid, and the shadow of a pixel cast on the detection plane is rectangular. As α decreases the shadow enlarges as it becomes blurred. As the Fresnel integral is an odd function, it is easy to verify that F_λ is even. Furthermore the extrema of $F_\lambda(\boldsymbol{U})$ are obtained for

$$U_x = \frac{\tau_{2x}}{\alpha_x^2} z_x, \quad U_y = \frac{\tau_{2y}}{\alpha_y^2} z_y, \tag{42}$$

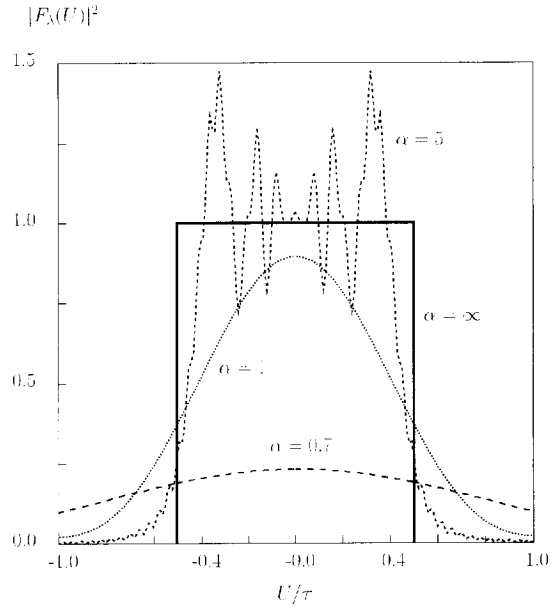

Fig. 5. Cross-section of the squared modulus of the Fresnel point spread function of a rectangular pixel.

where z_x and z_y are integers. Minima are obtained for odd z_x or z_y, and maxima for even z_x or z_y. The first minimum appears for $z = (1,0)$ along the X axis, and for $z = (0,1)$ along the Y axis. As the function F_λ is even, α_x^2/τ_{2x} measures approximately its width at half-maximum along the X axis. We take the coefficients α_x^2/τ_{2x} and α_y^2/τ_{2y} as measures of the diffraction strength. These have several equivalent expressions involving the different geometrical parameters, for instance

$$\frac{\alpha_x^2}{\tau_{2x}} = \frac{1}{\tau_{2x}} \frac{a_{2x}^2}{\lambda|d'|} = \frac{G}{\tau_{2x}} \frac{a_{2x}^2}{\lambda d} = G \frac{a_{2x} b_{2x}}{\lambda d}. \tag{43}$$

Coefficients α_x^2/τ_{2x} and α_y^2/τ_{2y} alone are not enough to estimate exactly the resolution, but provide rather a rough estimation. An exact assessment of the resolution requires the evaluation of the diffraction array V. The expression (33) of coefficients $V(\boldsymbol{q},\boldsymbol{q}')$ involves integration on both source and detection pixels. As a rule of the thumb, we have verified by numerical simulation that the smaller the pixel fill factor in both source and detection planes the higher the resolution. But conversely the energy losses increase with smaller pixels. Adopting the convention that diffraction coefficients $V(\boldsymbol{q},\boldsymbol{q}')$ with a modulus is 1000 times smaller than the central coefficient $V(\mathbf{0},\mathbf{0})$ are negligible, and for source and detection planes pixel fill factors close to unity, we obtained numerically the estimation of the size of array V shown in Table 1.

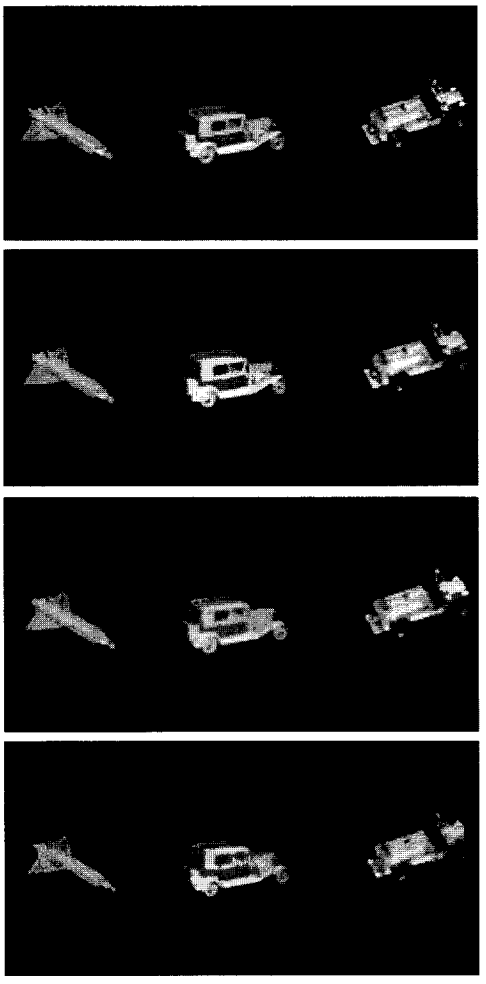

Fig. 6. Numerical simulation of the shadow $D[t_2]$ for source, intermediate and detection planes pixel fill factors close to unity. From top to bottom, $\alpha = \alpha_x = \alpha_y = \infty$ (no diffraction), $\alpha = 1.0$, $\alpha = 0.6$, and $\alpha = 0.4$.

Fig. 6 shows an example of a numerical simulation of the shadow $D[t_2]$, for some values of $\alpha = \alpha_x = \alpha_y$ and for $\tau_{2x} = \tau_{2y} = 1$. The source and detection planes pixel fill

Table 1
Approximate size of the 4D array V of diffraction coefficients as a function of parameters α_x^2/τ_{2x} and α_y^2/τ_{2y}, for source and detection planes pixel fill factors close to unity

	$5 \le \alpha_x^2/\tau_{2x} \le 1$	$1 \le \alpha_x^2/\tau_{2x} \le 0.2$	$0.2 \le \alpha_x^2/\tau_{2x} \le 0.1$
$5 \le \alpha_y^2/\tau_{2y} \le 1$	$5^2 \times 5^2$	$7^2 \times 5^2$	$9^2 \times 5^2$
$1 \le \alpha_y^2/\tau_{2y} \le 0.2$	$5^2 \times 7^2$	$7^2 \times 7^2$	$9^2 \times 7^2$
$0.2 \le \alpha_y^2/\tau_{2y} \le 0.1$	$5^2 \times 9^2$	$7^2 \times 9^2$	$9^2 \times 9^2$

factors are either equal to 1. The degradation of the shadow when compared to the original image as α decreases can be observed. Visually, this degradation looks like a blur, as it should. Note however that this is not a classical geometrical blur, since $D[t_2]$ is a quadratic transformation of image t_2. Indeed, a slight edge enhancement can be observed.

6. Conclusion

We have investigated the implications of pixelation in shadow casting systems. It follows from the analysis of purely geometrical properties of such systems that the pixel grids in the source, intermediate and detection planes must be identical up to a scale factor, and that the physical extent of the pixels causes a small linear blur, i.e. a convolution of the intensity of the second image with a 3 × 3 kernel. When diffraction is taken into account, and within the Fresnel approximation, the blur is a quadratic transformation of the amplitude of the second image. This quadratic blur involves a 4D array, whose coefficients depend on the geometrical set-up, the pixels shapes and the source spectrum. The extent of this array can be used to characterize the diffraction limited resolution. Our model can also be used for an efficient numerical simulation of pixelated shadow casting systems. We have emphasized on the common case of rectangular pixels and given practical examples of resolution estimation and shadow computation in this case.

Acknowledgements

This research was partly supported by the Direction des Recherches et Etudes Techniques (DRET) under contract No 92/352. The author wishes to thank gratefully Ph. Réfrégier, P. Chavel, J.-P. Huignard, D. Broussoux, G. Delaforest, S. Formont and J. Figue for helpful suggestions and discussions.

Appendix A. Incoherent PSF

Within the Fresnel approximation of diffraction [17], the incoherent point spread function of the system can be written as

$$H_\lambda(\boldsymbol{R}_1,\boldsymbol{R}_3) = A^2\left|\int_{\mathscr{P}_2} \mathrm{d}\boldsymbol{R}_2\, t_2(\boldsymbol{R}_2)\exp\left(\frac{i\pi}{\lambda d}|\boldsymbol{b}_2\odot\boldsymbol{R}_2-\boldsymbol{b}_1\odot\boldsymbol{R}_1|^2\right)\times\exp\left(\frac{i\pi}{\lambda p}|\boldsymbol{b}_2\odot\boldsymbol{R}_2-\boldsymbol{b}_3\odot\boldsymbol{R}_3|^2\right)\right|^2. \quad (A.1)$$

where A^2 is a constant that will be identified later. This equation expresses the propagation of a spherical wave emitted at point $\boldsymbol{R}_1$ in plane $\mathscr{P}_1$, diffracted in plane $\mathscr{P}_2$ by amplitude transmittance t_2 into spherical wavelets that reach detection point $\boldsymbol{R}_3$ in plane $\mathscr{P}_3$. Using the identity

$$\frac{(b_{2x}X_2-b_{1x}X_1)^2}{d}+\frac{(b_{2x}X_2-b_{3x}X_3)^2}{p} = \frac{(b_{3x}X_3-b_{1x}X_1)^2}{d+p} + \frac{(b_{2x}(X_2-\epsilon X_1-\epsilon' X_3))^2}{d'}, \quad (A.2)$$

and a similar identity for the Y axis, Eq. (A.1) becomes

$$H_\lambda(\boldsymbol{R}_1,\boldsymbol{R}_3) = A^2\left|\int_{\mathscr{P}_2}\mathrm{d}\boldsymbol{R}_2\, t_2(\boldsymbol{R}_2)\exp\left(\frac{i\pi b_{2x}^2}{\lambda d'}(X_2-\epsilon X_1-\epsilon' X_3)^2\right)\times\exp\left(\frac{i\pi b_{2y}^2}{\lambda d'}(Y_2-\epsilon Y_1-\epsilon' Y_3)^2\right)\right|^2. \quad (A.3)$$

Introducing $t_2(\boldsymbol{R}_2)=\sum_{\boldsymbol{n}} t_2(\boldsymbol{n})p_2(\boldsymbol{R}_2-\boldsymbol{n})$ into Eq. (A.3) we get

$$H_\lambda(\boldsymbol{R}_1,\boldsymbol{R}_3) = \left|\sum_{\boldsymbol{n}} t_2(\boldsymbol{n})\,F_\lambda(\epsilon\boldsymbol{R}_1+\epsilon'\boldsymbol{R}_3-\boldsymbol{n})\right|^2, \quad (A.4)$$

where

$$F_\lambda(\boldsymbol{U}) = A\int_{\mathscr{P}_2}\mathrm{d}\boldsymbol{R}_2\, p_2(\boldsymbol{R}_2)\exp\left(\frac{i\pi b_{2x}^2}{\lambda d'}(X_2-U_x)^2\right)\times\exp\left(\frac{i\pi b_{2y}^2}{\lambda d'}(Y_2-U_y)^2\right), \quad (A.5)$$

is the coherent Fresnel PSF in plane $\mathscr{P}_3$ created by a single pixel at the origin of plane $\mathscr{P}_2$. The constant A can be obtained by expressing the energy conservation as

$$\int_{\mathscr{P}_3}|F_\lambda(\boldsymbol{U})|^2\,\mathrm{d}\boldsymbol{U}=\int_{\mathscr{P}_2}|p_2(\boldsymbol{R}_2)|^2\,\mathrm{d}\boldsymbol{R}_2 = Sp_2, \quad (A.6)$$

that implies

$$A=\frac{S_2}{\lambda|d'|}. \quad (A.7)$$

We have thus obtained Eqs. (25) and (26).

Appendix B. Input–output relation

Upon inserting Eqs. (25) and (29) in Eq. (27) we get

$$\Phi_3(\boldsymbol{k}) = S_1 S_3 \int B(\lambda)\,\mathrm{d}\lambda \sum_{\boldsymbol{m}} Q(\boldsymbol{m},\boldsymbol{k}) T_1(\boldsymbol{m}) \times \sum_{\boldsymbol{n}} t_2(\boldsymbol{n}) \sum_{\boldsymbol{n}'} t_2^*(\boldsymbol{n}') \int_{\mathscr{P}_1} \mathrm{d}\boldsymbol{R}_1 \times \int_{\mathscr{P}_3} \mathrm{d}\boldsymbol{R}_3\, p_1(\boldsymbol{R}_1 - \boldsymbol{m})\, p_3(\boldsymbol{R}_3 - \boldsymbol{k}) \times F_\lambda(\epsilon \boldsymbol{R}_1 + \epsilon' \boldsymbol{R}_3 - \boldsymbol{n})\, F_\lambda^*(\epsilon \boldsymbol{R}_1 + \epsilon' \boldsymbol{R}_3 - \boldsymbol{n}'), \tag{B.1}$$

and Eqs. (30)–(32) are obtained by setting

$$\boldsymbol{q} = \boldsymbol{n} - \epsilon \boldsymbol{m} - \epsilon' \boldsymbol{k}, \quad \boldsymbol{q}' = \boldsymbol{n}' - \epsilon \boldsymbol{m} - \epsilon' \boldsymbol{k}.$$

Whatever the wavelength, and for a fixed geometry, the energy that is contained in the whole shadow must be constant and proportional to

$$\sum_{\boldsymbol{n}} D[t_2](\boldsymbol{n}) = \sum_{\boldsymbol{n}} \sum_{\boldsymbol{q}} \sum_{\boldsymbol{q}'} V(\boldsymbol{q},\boldsymbol{q}')\, t_2(\boldsymbol{n} + \boldsymbol{q})\, t_2^*(\boldsymbol{n} + \boldsymbol{q}'), \tag{B.2}$$

or in the limit of ray optics

$$\sum_{\boldsymbol{n}} \mathscr{G}[T_2](\boldsymbol{n}) = \sum_{\boldsymbol{n}} \sum_{\boldsymbol{q}} A(\boldsymbol{q})\, T_2(\boldsymbol{n} + \boldsymbol{q}). \tag{B.3}$$

Both quantities must be the same, since ray optics is obtained in the limit of short wavelengths. Assuming first $t_2(\boldsymbol{n}) = 1$ for all $\boldsymbol{n}$ yields

$$\sum_{\boldsymbol{q}} A(\boldsymbol{q}) = \sum_{\boldsymbol{q}} \sum_{\boldsymbol{q}'} V(\boldsymbol{q},\boldsymbol{q}'). \tag{B.4}$$

Then with $t_2(\boldsymbol{n}) = \delta_{\boldsymbol{n}}$, where δ is the Kronecker symbol that equals 1 if $\boldsymbol{n}$ equals 0 and 0 otherwise, we get

$$\sum_{\boldsymbol{q}} A(\boldsymbol{q}) = \sum_{\boldsymbol{q}} V(\boldsymbol{q},\boldsymbol{q}). \tag{B.5}$$

Combining Eqs. (B.4) and (B.5) we have that

$$\sum_{\boldsymbol{q}} \sum_{\boldsymbol{q}' \neq \boldsymbol{q}} V(\boldsymbol{q},\boldsymbol{q}') = 0. \tag{B.6}$$

Using a classical result of distribution theory, we have

$$\lim_{\lambda \to 0} \left[\frac{S_2}{\lambda |d'|} \exp\left(\frac{i\pi b_{2x}^2}{\lambda |d'|} (X_2 - U_x)^2 \right) \times \exp\left(\frac{i\pi b_{2y}^2}{\lambda |d'|} (Y_2 - U_y)^2 \right) \right] = \delta(\boldsymbol{R}_2 - \boldsymbol{U}), \tag{B.7}$$

and inserting into Eq. (25)

$$\lim_{\lambda \to 0} [F_\lambda(\boldsymbol{U})] = p_2(\boldsymbol{U}). \tag{B.8}$$

We then have

$$\lim_{\lambda \to 0} [V(\boldsymbol{q},\boldsymbol{q}')] = \int_{\mathscr{P}_1} \mathrm{d}\boldsymbol{R}_1 \int_{\mathscr{P}_3} \mathrm{d}\boldsymbol{R}_3\, p_1(\boldsymbol{R}_1)\, p_3(\boldsymbol{R}_3) \times p_2(\epsilon \boldsymbol{R}_1 + \epsilon' \boldsymbol{R}_3 - \boldsymbol{q})\, p_2(\epsilon \boldsymbol{R}_1 + \epsilon' \boldsymbol{R}_3 - \boldsymbol{q}'). \tag{B.9}$$

As the pixels p_2 are non-overlapping, the previous expression is different from 0 only if $\boldsymbol{q} = \boldsymbol{q}'$, and then

$$\lim_{\lambda \to 0} [V(\boldsymbol{q},\boldsymbol{q})] = A(\boldsymbol{q}),$$
$$\lim_{\lambda \to 0} [V(\boldsymbol{q},\boldsymbol{q}')] = 0 \quad \text{if } \boldsymbol{q}' \neq \boldsymbol{q}. \tag{B.10}$$

This shows that the diffraction shadow identifies with the geometrical shadow in the limit that the wavelength approaches 0.

References

[1] J.M. Robertson, Nature 152 (1943) 411.
[2] L. Bragg, Nature 154 (1944) 69.
[3] G.L. Rogers, Noncoherent optical processing (Wiley, New York, 1977).
[4] Y. Ichioka, J. Tanida, Proc. IEEE 72 (1984) 787.
[5] Y. Li, A. Kostrzewski, D.H. Kim, G. Eichmann, Optics Lett. 14 (1989) 981.
[6] A. Louri, Appl. Optics 14 (1989) 3264.
[7] I. Glaser, Information processing with spatially incoherent light, in: Progress in Optics XXIV, Ed. E. Wolf (North-Holland, Amsterdam, 1987) pp. 391–509 .
[8] E.L. Green, Appl. Optics 7 (1968) 1237.
[9] K. Raj, D.W. Prather, R.A. Athale, J.N. Mait, Appl. Optics 32 (1993) 3108.
[10] K. Raj, R.A. Athale, Appl. Optics 34 (1995) 1951.
[11] M. Gedziorowski, T. Szoplik, Optics Comm. 106 (1994) 167.
[12] M. Gedziorowski, J. Garcia, Optics Comm. 119 (1995) 207.
[13] V. Laude, P. Chavel, Ph. Réfrégier, Appl. Optics 35 (1996) 5267.
[14] M. Nieto-Vesperinas, Diffraction and scattering in physical optics (Wiley, New York, 1991).
[15] P.L. Jackson, Appl. Optics 6 (1967) 1272.
[16] M.A. Monahan, K. Bromley, R.P. Bocker, Proc. IEEE 65 (1977) 121.
[17] M. Born, E. Wolf, Principles of Optics (Pergamon Press, New York, 1980).
[18] B. Barakat, The calculation of integrals encountered in optical diffraction theory, in: The computer in optical research, Ed. B.R. Frieden (Springer, Berlin, 1980) pp. 35–80.
[19] I.S. Gradshteyn, I.M. Ryzhik, Table of Integrals, Series and Products (Academic Press, New York, 1980).